

Article

Permeable Membranes PUR/TETA and PUR/TEPA for CO₂ Capture Prepared with One-Step Electrospinning Technology

Jakub Hoskovec ^{1,*} , Pavla Čapková ¹ , Monika Vostiňáková ¹ , Petr Ryšánek ¹ , Pavel Kaule ² ,
Jonáš Tokarský ^{3,4} , Oldřich Benada ^{5,6}  and Vratislav Blechta ²

¹ Centre of Nanomaterials and Biotechnology, Faculty of Science, J. E. Purkyne University, Pasteurova 3632/15, 400 96 Usti nad Labem, Czech Republic

² Chemistry Department, Faculty of Science, J. E. Purkyne University, Pasteurova 3632/15, 400 96 Usti nad Labem, Czech Republic

³ Nanotechnology Centre, CEET, VSB-Technical University of Ostrava, 17. Listopadu 15/2172, 708 00 Ostrava, Czech Republic

⁴ Institute of Environmental Technology, CEET, VSB-Technical University of Ostrava, 17. Listopadu 15/2172, 708 00 Ostrava, Czech Republic

⁵ Department of Biology, Faculty of Science, Jan Evangelista Purkyne University, Za Valcovnou 1000/8, 400 96 Usti nad Labem, Czech Republic

⁶ Institute of Microbiology of the Czech Academy of Sciences, Videnska 1083, 142 20 Prague, Czech Republic

* Correspondence: jakub.hoskovec@ujep.cz

Abstract: A simple one-step technology of wire electrospinning is presented for the manufacturing of air-permeable CO₂-capturing membranes, easily transferable to industrial production lines. The design of the chemically-modified polyurethane nanofiber membranes for CO₂ capture was based on a combination of molecular modeling and technological experiments using one-step electrospinning (i.e., a modifying agent dissolved directly in a spinning solution). Polyurethane (PUR Larithane), chemically modified by TETA/TEPA amines, was used in the present study for the membrane design. Special attention was paid to two key parameters significant for the design of the functional unit, i.e., the CO₂ sorption capacity and air permeability which depended on the amine concentration. The optimal combination of these parameters was found for the PUR/TEPA membrane (5 wt.% of TEPA in spinning solution): the sorption capacity was 13.97 cm³/g with an air permeability of 0.020 m/s. Molecular modeling proved to be a valuable tool that helped to clarify, at the molecular level, the structure of chemically-modified nanofibrous membranes.

Keywords: CO₂ adsorption; electrospinning; polyurethane nanofibers; sorption capacity; solid supported adsorbent



Citation: Hoskovec, J.; Čapková, P.; Vostiňáková, M.; Ryšánek, P.; Kaule, P.; Tokarský, J.; Benada, O.; Blechta, V. Permeable Membranes PUR/TETA and PUR/TEPA for CO₂ Capture Prepared with One-Step Electrospinning Technology. *Fibers* **2022**, *10*, 100. <https://doi.org/10.3390/fib10110100>

Academic Editor: Mazeyar Parvinezadeh Gashti

Received: 10 October 2022

Accepted: 9 November 2022

Published: 16 November 2022

Publisher's Note: MDPI stays neutral with regard to jurisdictional claims in published maps and institutional affiliations.



Copyright: © 2022 by the authors. Licensee MDPI, Basel, Switzerland. This article is an open access article distributed under the terms and conditions of the Creative Commons Attribution (CC BY) license (<https://creativecommons.org/licenses/by/4.0/>).

1. Introduction

One of the most important and often rightly raised concerns today is the release and accumulation of carbon dioxide and other greenhouse gases into the atmosphere, which then changes the Earth's climate [1–3]. For this reason, the view of many research groups around the world is focused on the possibility of immediate actions against increasing CO₂ emissions through many ways of capturing it [4,5], including liquid media absorption technologies using chemisorption, such as amine-based solvents (the amine washing method) or ionic liquid (IL) physisorption [6]. Adsorption technologies using solid materials, which could again be classified as high-temperature chemisorbents (alkali metals or alkaline earth metal oxides) and low-temperature physisorbents (zeolites, carbon-based materials, metal organic frames (MOFs)), porous polymer networks (PPNs), and covalent organic structures (COFs) [6]; separation membrane technologies using, for example, nanofiber nonwoven membranes, mixed-matrix membranes (MMMs), facilitated-transport membranes (FTMs), etc. [6–8]. However, not all methods, whether the above or others, combine two very important and constantly balanced relationships between the efficiency of CO₂ sorption,

the energy intensity of the whole system, and the material associated with it. Specifically, the already mentioned amine scrubbing method is very efficient in terms of the amount of CO₂ captured, but on the other hand, its energy consumption is high [9]. For a specific example, according to Rochelle [10], with a completely standard setting of technology used in the field of coal-fired power plants, the value of the energy needed to capture a metric ton of CO₂ corresponded to 0.11 megawatt-hours.

In addition to this application disadvantage, due to the liquid form of amines, this technology is potentially dangerous for the health of the individual or the environment. Membrane technologies/materials are economically-, health-, and environmentally- friendly but are also inefficient at capturing CO₂, as described by Ho et al. [11]. In recent years, various nanofiber polymeric materials were prepared by electrospinning using a number of processes for the formation of CO₂-adsorbing membranes, including the impregnation with amines, MOFs, carbonization, and further activation. Zainab et al. [12] synthesized PS/PU nanofiber membranes with hierarchically porous structures, a high surface area of ~62 m²·g⁻¹, and a high CO₂ adsorption capacity of 1.64 mmol·g⁻¹ for the optimized membranes. In the next study, Abbasi et al. [13] and many more [14–22] developed a new amine-bearing nanofibrous adsorbent (electrospinning of s-PP, RIG of GMA, and amination with EA) for the removal of CO₂ with the highest CO₂ adsorption capacity of 2.87 mmol/g. Other amine-based materials have been reported elsewhere [23–38].

Most of the published methods employing the carbonization of polymeric nanofibrous materials achieved excellent sorption capabilities, which were further enhanced by subsequent activation (with steam or CO₂ activation [20,21]). The disadvantage of these technologies, in addition to the high number of technological steps, is the resulting sorption medium in the form of powders. This complicates the design of a functional unit operating in the waste gas stream. The present work is therefore focused on the development of permeable CO₂-adsorbing membranes based on chemically-modified polymer nanofiber membranes prepared with one-step electrospinning technology, i.e., the modifying agent is added directly to a spinning solution. For the spinning technology, we chose wire spinning technology (nanospider technology), which is easily transferable to industrial production lines.

For the nanofiber polymer matrix, we chose polyurethane (PUR larithane) as a suitable material due to its thermal and mechanical properties and also for the flexibility of the polymer chains, which has a large number of diols and isocyanates interacting with each other through so-called carbamate interactions [39,40]. Triethylenetetramine and tetraethylenepentamine amines were chosen as the modifying agents for CO₂ sorption. Despite a large number of reported results, there is still a significant amount of space for studying the essential phenomena associated with the chemical functionalization of nanofibers and the effects of modifying agents on the morphology, structures, properties, and functions of membranes. The aim of this work is a simple one-step technology for the preparation of air-permeable CO₂-adsorbing membranes, transferable to industrial lines. The one-step technology used in this work has three main advantages:

- The modifying agent is dissolved in a spinning solution, and no subsequent treatment is necessary;
- This technology does not destroy the porosity and air permeability of the membrane as in the case of various after-treatment procedures;
- Our air membrane is easy to design as a cascade sorption unit working in the stream of gas.

2. Materials and Methods

2.1. Materials and Spinning Solution

Polyurethane (PUR)–Larithane AL 286 was purchased from CoimGroup, dimethyl-formamide 99% (DMF) (MW = 73.10 g·mol⁻¹) was purchased from AvantorTM, triethylenetetramine (TETA) (MW = 146.23 g·mol⁻¹ (anhydrous basis)), and tetraethylenepentamine (TEPA) (MW = 189.30 g·mol⁻¹) were purchased from Sigma-Aldrich. PUR (Larithane AL 286)/DMF stock solution was prepared at a 45% concentration (*w/w*). This starting

solution was subsequently modified with selected amines, namely TETA, and TEPA, at two concentrations corresponding to 1 and 5 wt.% as follows: while stirring at 300 rpm without added heating (at room conditions), the appropriate amount of modifier was added gradually. The solutions thus prepared were allowed to stir for 24 h to achieve complete homogenization.

2.2. Spinning Conditions

Nanospider electrospinning technology (needle-free electrospinning technology) using a wire as a spinning electrode was used. The most used technology using free-surface spinning electrodes is collectively assigned to the device called Nanospider [41], which in its earliest form worked with a spinning electrode in the form of a conductive cylinder, later replaced by wire to control the fiber diameter better. Nanofiber membranes were prepared using wire electrospinning technology with a commercial Nanospider™ NS 1WS500U device from Elmarco (Liberec, Czech Republic).

One-step technology was used in the present work, which meant that the modifying agents (the TETA and TEPA amines) were dissolved in a spinning solution. The solutions were then dispensed in an amount of 20 mL into a pre-prepared apparatus of the dosing mechanism, the so-called slider, with a used slit of 0.6 mm. During the spinning process, the same process, the parameters always prevailed for each wt.% of starting amine modifying solution used. These parameters are closely related to the electrospinning process and significantly influence the resulting properties of the electrostatically prepared product [42]. In the case of this work, the following parameters were used: an applied voltage of 50/20 kV, a working distance of 150 mm, a cartridge speed of 400 mm/s, and a winding speed of spunbond base material (PP) of 40 mm/min. Ambient conditions were maintained at 25 °C and 22% relative humidity with an industrial dryer.

2.3. Membrane Characterization Methods

The prepared samples of the PUR/TETA and PUR/TEPA membranes were characterized with a series of analytical methods: scanning electron microscopy (SEM), X-ray diffraction (XRD) analysis, hydrophobicity, electrokinetic analysis of surface chemistry, NMR analysis, and air permeability measurements. Atomistic molecular simulations were used to elucidate the interactions of polymer amines. Finally, CO₂ sorption tests were performed to determine the sorption capabilities of the formed nanofibrous materials with respect to CO₂. SEM analysis without high resolution was performed using the VEGA3 instrument (Tescan, Brno, Czech Republic) in software where the average values of the nanofiber diameters were also measured directly. All images were taken at a constant value of the acceleration potential of 20 kV in the resolution mode with the detector set to secondary electrons (SEs). A magnification of 10,000× was used. For the analysis itself, the samples were sputtered on the sputtering station Q 150T ES (Quorum Technologies Ltd., Ringmer, UK) of 20 nm gold for the optimal SE yield. The manual measurements of the nanofiber diameters (MMD) were supported by the automatic evaluation of the individual nanofiber diameters performed using the DiameterJ plugin in the FIJI image processing software [43]. Based on the facts described in Section 3.1, a high-resolution electron microscopy (HRSEM) analysis was also performed using an FEI Nova NanoSEM device (FEI, Brno, Czech Republic) for the specific modification of PUR/TEPA 5 wt.%. The samples for the analysis itself were plated with a 3 nm layer of platinum. The images were taken at an accelerating voltage of 3 kV in the concentric backscatter electron (CBS) mode of the detector. A magnification of 50,000× was used.

The XRD analysis was performed using a Philips powder diffractometer, PANalytical, type X'pert PRO (Malvern Panalytical Ltd., Malvern, UK) in a symmetrical Bragg-Brentano arrangement at an angular range of 5–40° 2θ. The membrane samples were layered to achieve the best possible diffracted radiation intensity and, at most, on the non-diffractive silicon wafer so that the diffraction plane was parallel to the plane of the membrane. The radiation used was Cu Kα (λ = 1.5418 Å), and a Ni Kβ filter was used.

Detector 0 D proportional, a solid $1/2^\circ$ divergence clone, and a parabolic Goebel mirror for a parallel X-ray beam were included in the incident beam. The voltage and current for the X-ray were 40 kV and 30 mA. The diffraction records were evaluated using HighScore Plus software with the PDF-2 database.

The goniometric analysis was performed using a Krüss drop shape analyzer (DSA30B, KRÜSS GmbH, Hamburg, Germany) to determine the contact angle and thus obtain information on the hydrophilicity and hydrophobicity surface properties of the nanofiber-modified membranes with respect to the unmodified membranes of “pristine” polyurethane. The water contact angle was measured under constant laboratory conditions.

To control for the presence of modifiers on the nanofiber surfaces, we used electrokinetic measurements of zeta potential. The zeta potential was determined using a SurPASS electrokinetic analyzer (Anton Paar, Austria). A pair of samples with the same surface area was attached to holders (2×1 cm) in a cell with an adjustable gap (approximately 100 μm) in the presence of the electrolyte 0.001 mol/dm³ KCl at room temperature, an atmospheric pressure, and a constant of pH 6.7. The results were evaluated using the streaming current method and the Helmholtz–Smoluchowski equation [44–47].

The liquid and solid phase nuclear magnetic resonance (NMR) spectra of Larithane were measured with a JNM-ECZ400R spectrometer (JEOL Ltd., Tokyo, Japan) operating at a resonance frequency of 400 MHz for the hydrogen nuclei and 100 MHz for the carbon nuclei. The input commercial polymer solution was measured for the first time in the liquid phase (CDCl₃ and DMSO-*d*₆ solvents) without any modifications. Secondly, DMF was evaporated from 30 cm³ of the Larithane solution using a high vacuum (0.02 Torr at 40 °C for 8 h), and then the sample was measured in DMSO-*d*₆. Fibrous electrospun Larithane was also measured as a liquid phase sample when dissolved in DMSO-*d*₆. The chemical shifts of the ¹H and ¹³C spectra were referenced to DMSO-*d*₆. The assignment of the ¹H and ¹³C signals in the liquid was based on the findings from homo- and hetero-nuclear experiments, where correlations of ¹H and ¹³C nuclei were observed (e.g., ¹H-¹H COSY, ¹H-¹H TOCSY, ¹H-¹³C HMQC, and ¹H-¹³C HMBC).

The fibrous electrospun polymer was characterized with solid phase NMR. This nanofabric textile was cut into small pieces (approximately 4 × 4 mm) and packed into a ZrO₂ solid-state NMR rotor with an outer diameter of 3.2 mm. All ¹³C NMR spectra were measured at a magic spinning angle of 15 kHz. Chemical shifts of the ¹³C nuclei were measured by cross-polarization (CP MAS) with a relaxation delay of 5 s and 1000 scans. For the quantitative comparison, ¹³C NMR spectra were also measured with single-pulse sequences with decoupling during the acquisition, relaxation delays of 30 s and 60 s, and both with 1000 scans. The last two experiments provided identical results, which ensured their quantitative accuracy. The ¹H spectra were also experimentally measured at rotational frequencies of 0 kHz, 5 kHz, and 15 kHz at a magic angle.

The air permeabilities of the resulting membranes were analyzed on a device designed to determine this parameter from Polymertest (Otrokovice, Czech Republic). The measurements were performed in accordance with the standardized procedure defined by the ČSN EN ISO 9237 for the determination of the permeability of fabrics to air. Parameters, such as a test area of 20 cm² and a pressure gradient of 100 Pa, were constant during the measurements. The tests for the individual membranes were repeated ten times under the same conditions, always at a place where no measurement had been performed before.

The volume of carbon dioxide was determined with a CO₂ adsorption isotherm. The samples were degassed at room temperature for 24 h. After that, the adsorption and isotherms were recorded with carbon dioxide using a gas adsorption instrument (Autosorb iQ, Anton Paar, Austria). All the samples were characterized 3 times with an experimental error of 5%. The maximum adsorbed amount of CO₂ was calculated using the non-local density functional theory (NLDFT) model provided by Autosorb software.

The PUR chain chemical structure obtained with the NMR analysis was used in the docking calculations performed in the materials studio (MS) modeling environment (Biovia). Models of PUR, TETA, and TEPA were optimized in the MS/Forcite module using

the COMPASS force field [48], which assigned the parameters and charges of atoms. A smart algorithm (50,000 steps) was used for the geometry optimization with convergence criteria $\Delta E = 1 \times 10^{-4}$ kcal·mol⁻¹, $\Delta F = 5 \times 10^{-3}$ kcal·mol⁻¹·Å⁻¹, and $\Delta l = 5 \times 10^{-5}$ Å. The optimized PUR and TETA (or TEPA) molecules represented the base and screen, respectively, in the docking calculations performed in the MS/Blends module. The essence of docking is the generation of a large number of base-screen pairs (1,000,000 mutual positions were generated for each pair of molecules) and the determination of the interaction energy (E_{int} ; kcal/mol) of both molecules according to the equation,

$$E_{int} = E_{PUR/amine} - E_{PUR} - E_{amine}$$

where $E_{PUR/amine}$ (kcal/mol) is the total potential energy of the base-screen pair, E_{PUR} (kcal/mol) is the total potential energy of the base, i.e., PUR, and E_{amine} (kcal/mol) is the total potential energy of the screen, i.e., TETA or TEPA. The more negative the E_{int} value, the stronger the base-screen interaction.

3. Results and Discussion

3.1. Fiber Morphology, Air Permeability, and CO₂ Sorption Capacity

By comparing the SEM images in Figure 1, we could conclude that both amines led to changes in fiber morphology, i.e., significant decreases in fiber diameters (Table 1) and the straightening of the fibers (Figure 1b,d). With increasing amounts of applied amine, one can see a higher concentration of defects in the form of spindle fibers and continuous layers of material (Figure 1c,e). This negative effect of amines on the fiber structure is more pronounced in the case of the TETA amine. These changes in fiber morphology, and consequently, in membrane structures, are due to the chemical modifications that resulted in significant increases in air permeability in Table 1, measured under the standard conditions of a test area of 20 cm² and a constant pressure gradient of 100 Pa.

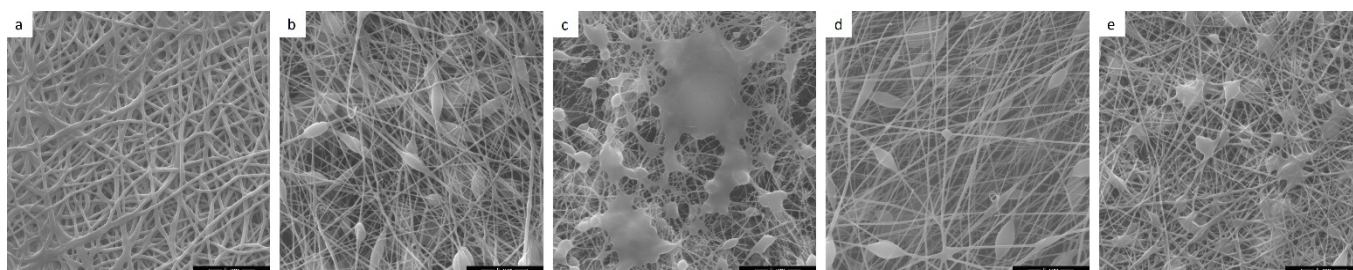


Figure 1. Original SEM images (a) pristine PUR; (b) PUR/TETA (1 wt.%); (c) PUR/TETA (5 wt.%); (d) PUR/TEPA (1 wt.%); (e) PUR/TEPA (5 wt.%).

Table 1. Average values of the nanofiber diameters (in nm) obtained in the MMD measurements and air permeability for the pristine PUR membrane and the TETA- and TEPA-modified amine membranes (1 and 5 wt.%) and the CO₂ sorption capacity in g/cm³ (third column).

Sample	MMD Nanofiber Diameter (nm)	Air Permeability (m/s)	CO ₂ Adsorbed Volume (cm ³ /g)
PUR	290 ± 37	0.002 ± 0.0002	2.7 ± 0.9
PUR/TETA (1 wt.%)	170 ± 24	0.05 ± 0.004	8.1 ± 1.9
PUR/TETA (5 wt.%)	164 ± 35	0.13 ± 0.02	8.09 ± 2.0
PUR/TEPA (1 wt.%)	174 ± 40	0.08 ± 0.01	6.8 ± 1.8
PUR/TEPA (5 wt.%)	166 ± 45	0.02 ± 0.003	13.9 ± 2.3

Table 1 summarizes the values of the fiber diameters, air permeabilities, and CO₂ sorption capacities for the measured samples, and it is evident that the chemical modifications increased the air permeabilities. It can be seen that the chemical treatment led

to a significant increase in the sorption capacity and, at the same time, an increase in air permeability compared to the pure PUR membrane. The maximum sorption capacity for the PUR/TEPA sample (5 wt.%)~13.9685 cm³/g was accompanied by a reduction in air permeability compared to other modified samples (Table 1). Therefore, a more demanding high-resolution SEM analysis (HRSEM) was performed for the PUR/TEPA samples, which revealed other interesting features of the membrane structure (Figure 2). The PUR nanofibers modified by the amines showed a tendency to stick to each other in bundles, and at higher concentrations, these bundles produced continuous surfaces. This behavior was not observed for short amines or other modifiers [49–51] and indicated the importance of the interaction energy polymer-modifier and modifier-modifier on the membrane structure. Therefore, we used molecular modeling (force field calculations) to analyze the intermolecular interactions in the PUR/TETA(TEPA) samples and to elucidate the effect observed in the HRSEM analysis (Figure 2).

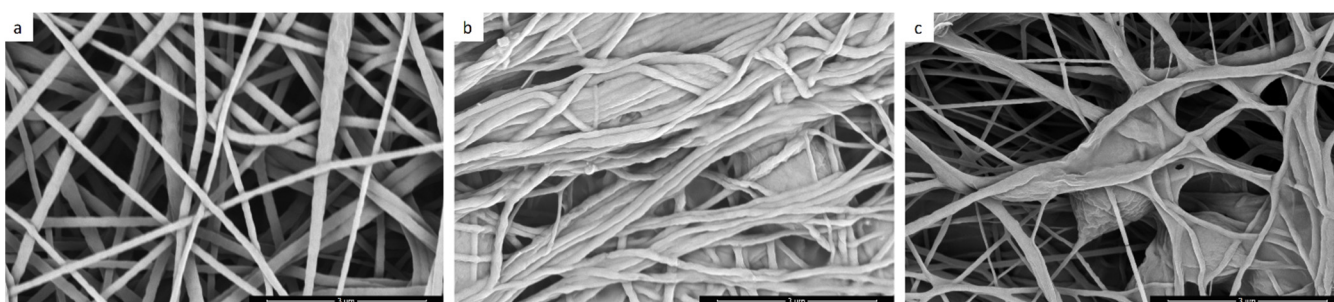


Figure 2. HRSEM images (a) pristine PUR without the occurrence of glued parallel fiber bundles or fused bands and layers; (b) PUR/TEPA (1 wt.%). A distinct characteristic feature of this sample is parallel bundles of fibers alternating with an irregular network; (c) PUR/TEPA (5 wt.%). After increasing the TEPA concentration to 5 wt.%, the individual fibers were fused into continuous strips and layers.

When comparing the CO₂ sorption capacities summarized in Table 1, the PUR/TETA and PUR/TEPA samples show different behaviors regarding the dependence of the sorption capacity on the amine concentration. While the increase in the TETA concentration did not lead to an increase in the sorption capacity of PUR/TETA, in the case of PUR/TEPA, the increase in concentration from 1 to 5 wt.% led to a double increase in sorption capacity.

3.2. XRD Analysis

The XRD structure analysis confirmed the crystallization of PUR during the spinning process (Figure 3). The diffraction profile at 2θ~20° corresponds to the parallel arrangements of the PUR chains in the fiber axis. This position of the main peak for PUR Larithane is shifted to a lower angle in comparison with the XRD profiles for electrospun polyamide 6 [49,51] and polyvinylidene fluoride [50], indicating the higher space requirement for PUR Larithane chains due to their larger volume (isophorone diisocyanate and one hexane-1,6-diol). Electrospun membrane samples are always strongly textured, which means that the diffraction profiles corresponding to the crystallographic planes perpendicular to the fiber axis are missing. In addition, the large width of the diffraction profiles shows very small PUR crystallites, which means no observable reflections were present at high 2θ angles. The intensity of the XRD profiles decreased with an increasing amine concentration, as the amount of crystalline PUR decreased in samples due to the lower fiber diameters. In the case of the PUR/TETA samples with 5 wt.% of TETA, the diffraction profile exhibited additional peaks corresponding to crystalline TETA. The crystallization tendency of TETA affected the surface morphology of the modified fibers and reduced the values of the sorption capacity for PUR/TETA (5 wt.%) in comparison with PUR/TEPA (5 wt.%).

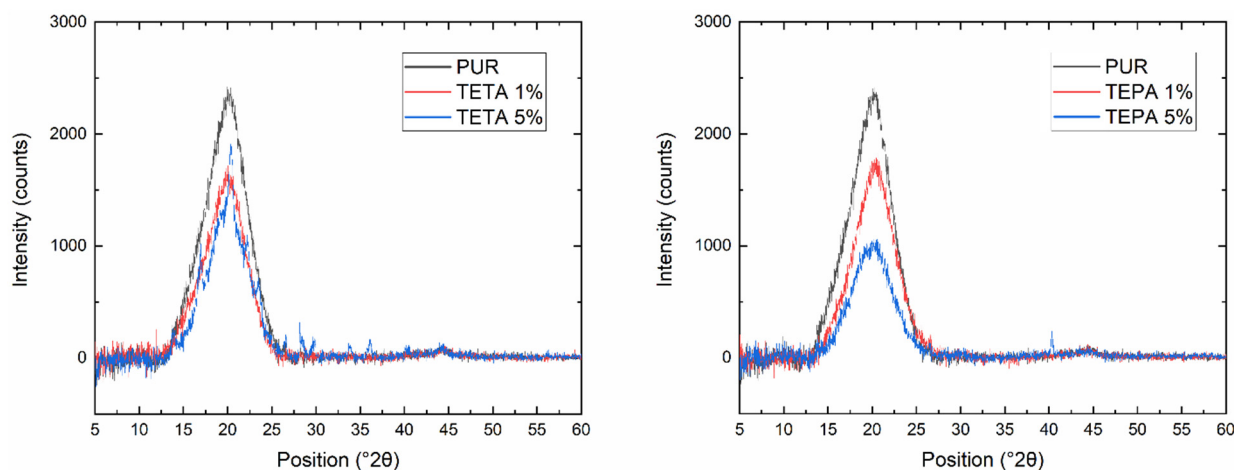


Figure 3. Diffractograms (CuK α) comparing the structural characteristics of the unmodified PUR membrane with the membranes modified with amines TETA (**left**) and TEPA (**right**).

3.3. Surface Chemistry of the PUR/TETA(TEPA) Membranes

The measurements of the contact angle and zeta potential provide the first information on the changes in surface chemistry due to nanofiber modifications and confirm the presence of a modifying substance on the surface of the fibers, which is a key condition for their functionality. This verification is especially important for one-step technology when the modifying substance is directly in the spinning solution, and the additive molecules could be closed inside the fibers. Although hydrophobicity and zeta potential alone are not interesting from the point of view of CO₂ sorption, they indicate the presence of amines on the fiber surface.

The values of the contact angles in Table 2 changed significantly as a result of the chemical modifications with TETA and TEPA, confirming the presence of amines on the surface of the nanofibers. The 5 wt.% concentration of amines led to a decrease in the contact angle to zero, which meant that the amine molecules were mainly on the surface of the fibers.

Table 2. Static contact angles and zeta potentials for all the membranes tested.

Sample	Static Contact Angle (°)	Zeta Potential (mV)
PUR	100 ± 7	−35.28 ± 0.1
PUR/TETA (1 wt.%)	120 ± 3	−6.72 ± 0.3
PUR/TETA (5 wt.%)	0	0.71 ± 0.4
PUR/TEPA (1 wt.%)	129 ± 10	30.34 ± 1.5
PUR/TEPA (5 wt.%)	0	0.39 ± 0.9

The presence of amines on the surface of the fibers also changed the values of the zeta potentials; however, there is another important factor influencing the zeta potential, which is, first, the roughness of the surface and, second, the location of the modifier. These could be both on the surface and inside the fibers, and therefore the dependence of the zeta potential on the concentration of the amine component does not show a monotonic course. Both the contact angle and zeta potential measurements confirmed the change in surface chemistry due to the chemical modifications by amines.

As the zeta potential is affected by the two factors mentioned above, there is no strong correlation between the columns of the values in Table 2, especially in the case of the 5 wt.% TETA modifying agent, as TETA tended to crystallize, as one can see from Figure 3. This led to inhomogeneous nanofiber surface coverage resulting in higher surface roughness.

3.4. PUR-TETA(TEPA) Interactions and Effect on the Membrane Structure and Properties

To understand the interactions of PUR with amines at the molecular level, we combined the NMR analysis with molecular modeling using force field calculations.

The PUR Larithane sample was measured in CDCl_3 and $\text{DMSO-}d_6$. The ^1H NMR chemical shifts (7.92, 2.86, and 2.79 ppm) of a commercial sample dissolved in CDCl_3 (not shown) revealed that dimethylformamide (DMF) was used as the solvent for the polyurethane polymer. Figure 4A shows the ^1H NMR spectrum of the Larithane sample in $\text{DMSO-}d_6$ with DMF evaporated. Three multiplets with characteristics splitting into one triplet (4.03 ppm), one quintet (1.57 ppm), and a multiplet at 1.31 ppm were unambiguously detected, indicating the presence of a linear dialcohol chain. The COSY experiment (not shown) proved three bond $^1\text{H-}^1\text{H}$ connections between the peaks at 4.03 ppm and 1.57 ppm and also a connection between the peaks at 1.57 ppm and 1.31 ppm. The triplet with a shift of 4.03 ppm was assumed to signal $-\text{CH}_2\text{O}-$ groups and the signals with shifts of 1.57 and 1.31 ppm were the $-\text{CH}_2-$ groups from the inner part of the chain.

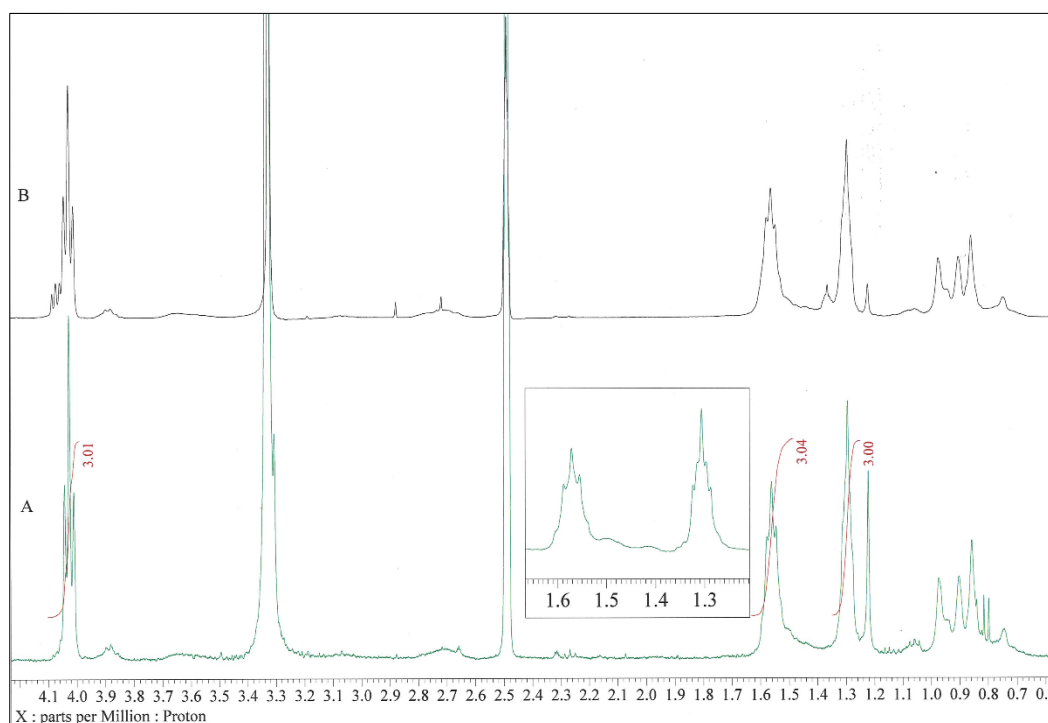


Figure 4. ^1H NMR of (A) commercial Larithane after distillation of DMF in a deep vacuum with a better resolution of the multiplets at 1.31 and 1.57 ppm confirmed quintet splitting, and (B) the fibrous nanotextile of Larithane after electrospinning. Both of the polymers were dissolved in $\text{DMSO-}d_6$.

The integral values of the signals with respect to the signals split by the homonuclear coupling interaction made it clear that each double signal represented the $-\text{CH}_2-$ groups of hexane-1,6-diol. The peaks in the range of 0.7–1.0 ppm could be assigned as the methyl groups in the isophorone units. Unfortunately, despite all efforts (Section 2.3), the remaining wide ^1H peaks of isophorone were difficult to observe and could not be reliably assigned.

^{13}C NMR spectra were measured with the APT experiment (Figure 5). Only the DMF signals, the $-\text{CH}-$ groups of the hexane-1,6-diol chain (67.59 ppm, 28.37 ppm, and 25.20 ppm), and the $-\text{C}=\text{O}$ group signal (155.15 ppm) could be unambiguously detected. The HMBC experiment indicated a $-\text{CH}_2-\text{O}-\text{C}=\text{O}$ bond between the hexane-1,6-diol unit and the carbonyl group. The other peaks were only hints; the reason for this is the large width of the lines from the less flexible part of the sample.

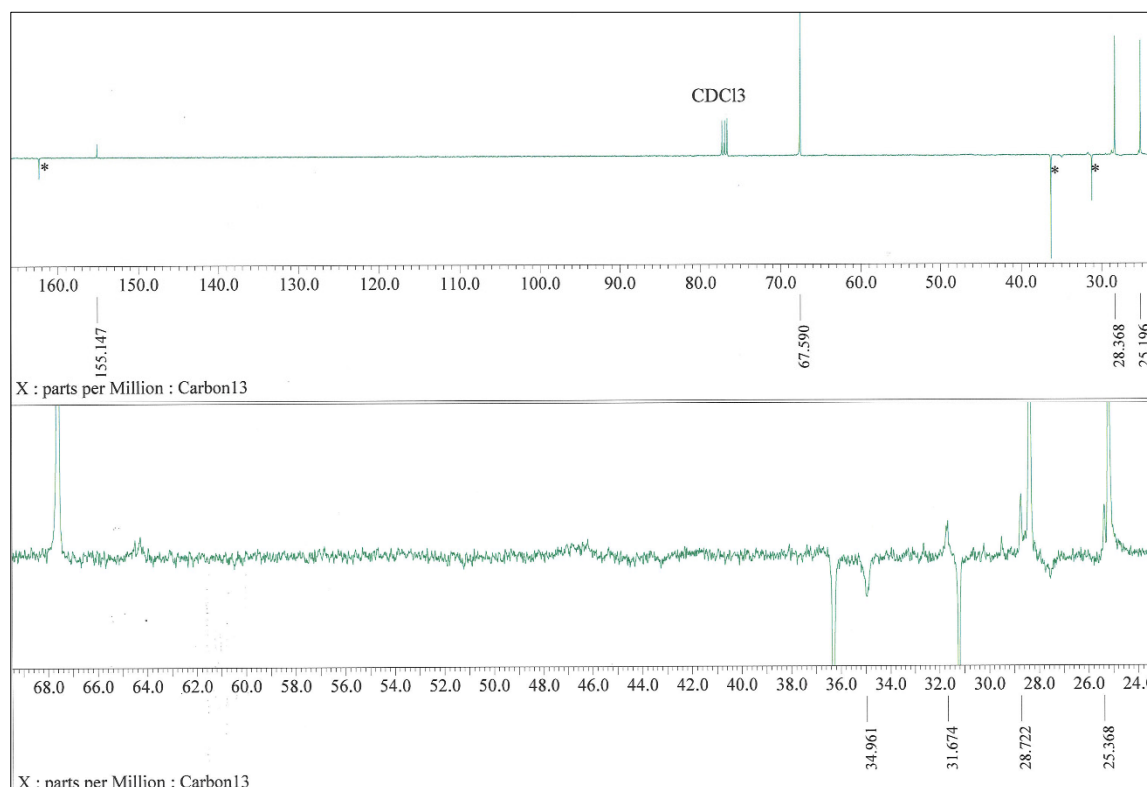


Figure 5. ^{13}C APT NMR spectrum of Larithane in CDCl_3 . The upward peaks belong to the $-\text{CH}_2-$ and C carbons, while the downward peaks belong to the $-\text{CH}$ and $-\text{CH}_3$ carbons. The DMF signals are marked with an asterisk (*).

The solid-state ^{13}C NMR analysis of the nanofabric textile Larithane, measured with a single pulse, quantitatively (Figure 6A), brought conspicuously sharp peaks corresponding to the $-(\text{C}=\text{O})-$ group (161.33 ppm) and all three different $-\text{CH}_2-$ groups bound to hexane-1,6-diol (73.56 ppm, 34.76 ppm, and 31.51 ppm). These peaks belonged to the moving part of the sample, i.e., the $-(\text{C}=\text{O})-\text{O}-(\text{CH}_2)_6-\text{O}-(\text{C}=\text{O})-$ fragment. At the same time, under these peaks (i.e., at the same or close frequency), wide peaks corresponding to more rigid parts of the sample are observed. The integral of the $-(\text{C}=\text{O})-$ peaks took place at a ratio of 1:1. Within the other peaks, it was difficult to quantify the area to integral ratio. The reduced flexibility of the aliphatic chains present in the structure of the polymer was verified by comparison with the ^{13}C spectra measured with cross-polarization. Cross-polarization generally favors signals of rigid carbons over flexible carbons. The cross-polarization spectra (Figure 6B) provided a stronger signal of the rigid part, and the signal from the moving part (161.32 ppm, 73.50 ppm, 34.69 ppm, and 31.51 ppm) was significantly suppressed. The wide peaks in the 45–60 ppm range probably belonged to nitrogen-bound carbon, while the broad peaks in the 38–45 ppm range and the peaks in the 25–38 ppm range below the sharp hexane-1,6-diol signals appeared to include signals from the remaining Larithane groups.

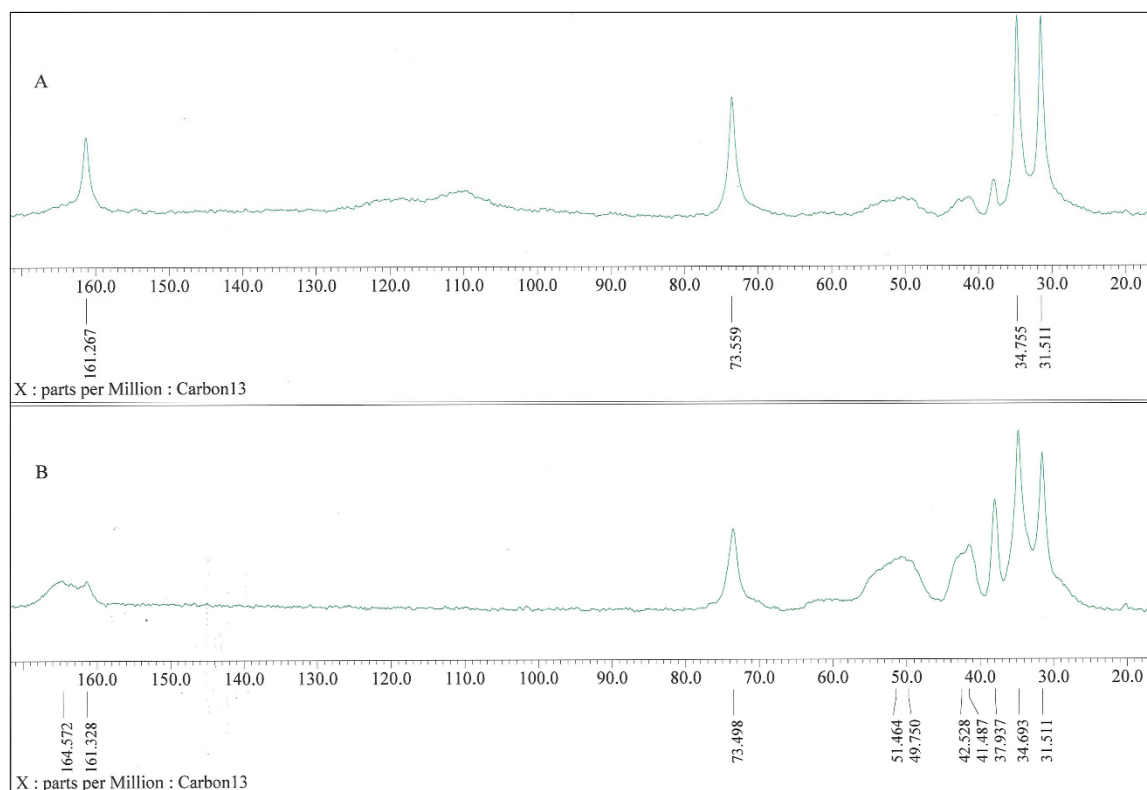


Figure 6. ^{13}C NMR spectrum measured in the solid-state: (A) single-pulse and (B) cross-polarization. The broad signal in the region 100–130 ppm in (A) is due to the Teflon spacers inserted into the spinner.

The ^1H solid-state spectra also showed that there was a decently flexible part in the sample and a much more rigid part: the spectrum contains a very wide peak (over 100 ppm) corresponding to a rigid part while the relatively narrow peak corresponding to the $-\text{CH}_2-$ groups of hexane-1,6-diol was superimposed on it even at zero spinning. At 5 kHz and 15 kHz, this peak split into two peaks at an integral ratio of 1:2, and the first corresponding $-\text{CH}_2-\text{O}-$ group and the second peak in the spectrum were close to the internal $-\text{CH}_2-$ groups. The solid-phase hetero-correlation of $^1\text{H}-^{13}\text{C}$ demonstrated that the $-\text{CH}_2-$ groups belonged to hexane-1,6-diol. The most interesting evidence was provided by a comparison of the input commercial Larithane proton spectra (Figure 4A) with the fibrous nanotextile (Figure 4B), both dissolved in $\text{DMSO}-d_6$. This spectrum proved that the polymer chain structure did not change during the electrospinning process. We did not find any such comparable results to discuss.

3.5. Molecular Modeling of the PUR-Amine Interactions

Based on the PUR structure determined with the NMR spectrum, one segment of the model chains consisted of one isophorone diisocyanate (the solid part) and one hexane-1,6-diol (the soft part) (Figure 7). A number of PUR chains with different numbers of segments were built, and the E_{int} values for TETA and TEPA with each of these chains were determined.

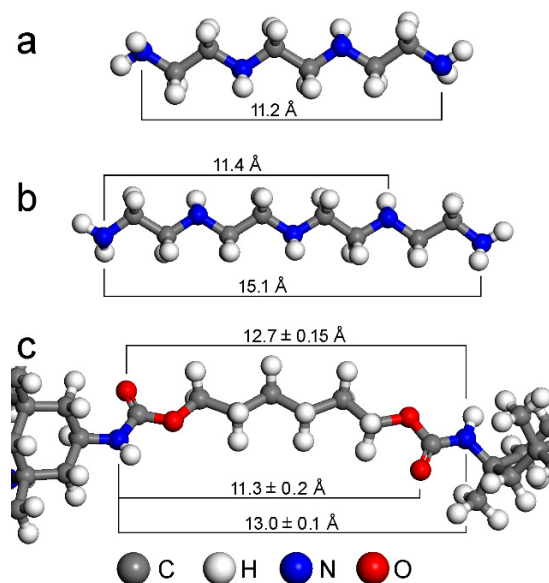


Figure 7. Functional groups' distances in geometry optimized (a) TETA, (b) TEPA, and (c) PUR models used for the docking calculations. In the case of PUR, all segments in all PUR models were measured, and the average distance values, along with the standard deviations, were determined.

The predominant component of the interaction energy of PUR-TETA/TEPA belonged to the hydrogen bonding between the functional groups on both of the interacting subjects, where the key factor was the distance of the functional group pairs in both the amine and PUR chains (Figure 7).

The structural similarity of the distances of the functional groups in the PUR and TETA(TEPA) structures drove the amines to energetically advantageous positions, more or less parallel to the PUR chain (Figure 8). Figure 8 illustrates two models for two extreme mutual positions of the PUR and amines, corresponding to the maximum absolute values of the interaction energies for the parallel- and cross-positions. A large number of functional groups guarantees considerable interaction energies even for cross-positions and provides a chance to connect the chains and nanofibers to each other, i.e., to facilitate the cross-linking of the membrane and its subsequent mechanical strengthening. Consequently, the models containing two PUR chains (78 segments each) and the number of amines corresponding to the amount provided by weight percentage (1 or 5 wt.%) were prepared for energy optimization. The models containing amines exhibited higher absolute values of interaction energies compared to models containing only two PUR chains without amines (Table 3). For 1 wt.% of amine, ~4 and ~3 molecules of TETA and TEPA, respectively, belonged to two PUR (78 segments) chains. For 5 wt.% of amine, ~18 and ~14 molecules of TETA and TEPA, respectively, belonged to two PUR (78 segments) chains.

Table 3. Models of two PUR chains (78 segments each) with different amounts of amines expressed by the number of molecules and weight percentages. The interaction energies (E_{int}) of two PUR chains with different amounts of amines are provided in the third column (E_{int} values for the same models without amines are provided in parentheses).

Sample	Amine (wt.%)	E_{int} (kcal/mol)
2PUR (78 seg)	0.00	-1959 ± 21
2PUR (78 seg) + 4TETA	1.13	-2152 ± 32 (-1977 ± 25)
2PUR (78 seg) + 3TEPA	1.10	-2153 ± 30 (-1939 ± 20)
2PUR (78 seg) + 18TETA	4.91	-3038 ± 47 (-1951 ± 22)
2PUR (78 seg) + 14TEPA	4.94	-2982 ± 41 (-1971 ± 22)

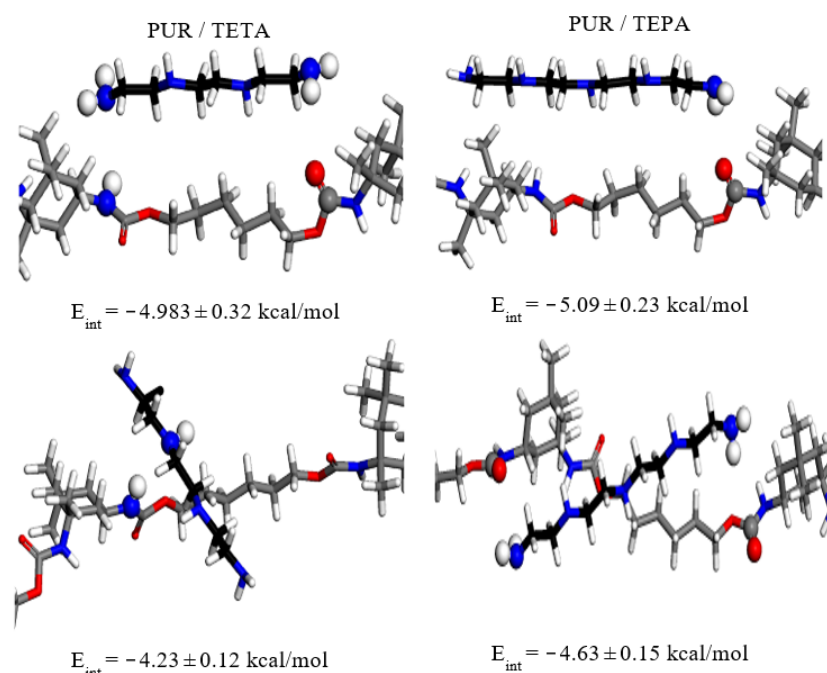


Figure 8. Mutual positions of PUR/TETA/TEPA corresponding to their maximum interaction energy for two extreme mutual positions, i.e., parallel and crossed. The atoms of the functional groups sharing hydrogen bonds are displayed as balls. For clarity, the carbon atoms in the amines are black.

Table 3 shows that models containing two PUR chains (78 segments each) and the number of amines corresponding to the amount given by weight percentage (1 or 5 wt.%) exhibited lower E_{int} compared to models containing only two PUR chains without amines (Table 3). For 1 wt.% of amine, ~4 and ~3 molecules of TETA and TEPA, respectively, belonged to two PUR (78 segments) chains. For 5 wt.% of amine, ~18 and ~14 molecules of TETA and TEPA, respectively, belonged to two PUR (78 segments) chains (Table 3). The decrease in the E_{int} (i.e., the enhanced strength of interactions) compared to the models containing only two PUR chains is evident. Table 3 clearly shows that the presence of amines on the PUR fiber surfaces increased the interaction energies of the fibers and explains the sticking of fibers observed with the HRSEM (Figure 2).

4. Conclusions

Many CO₂ sorbents reported in the literature were published and patented mainly in the form of powdered carbonized materials or non-porous films. As reported in the literature, these materials showed a much higher sorption capacity than our achieved value of 13.9 cm³/g for the PUR/TEPA sample (5 wt.%). However, even with these materials with large sorption values, there is a substantial practical limitation. It is precisely the powder or thin film form of such materials, the preparation of which involves multi-step procedures, which renders the technology more complicated and more expensive.

Sorption membranes are prepared with a similar technology, which means that electrospun nanofibers modified with different types of amines and MOFs reported in [12,13,18,52–54] exhibited comparable or much higher sorption capacities in the range 11.6–66.8 cm³/g. However, all these cited works used multi-step technology (more than one technological step). Therefore, the benefit of our one-step technology is its simplicity, preservation of air permeability, low cost, and easy transfer to industrial production lines. Taking into account these benefits, we must say that our sorption capacity is comparable with many other multi-step technologies, which always destroy the air permeability and complicate the design of functional sorption units.

The goal of this work was to prepare an electrospun membrane for CO₂ sorption that is air permeable. The combination of these two properties, i.e., the maximum CO₂ sorption capacity and air permeability, would significantly simplify the design of functional units

for practical use. Another important requirement is the one-step spinning technology, i.e., modifying substances directly in the spinning solution so that no subsequent technological steps are necessary. The sample PUR/TEPA (5 wt.%) was shown to meet this condition with a sorption capacity 5 times higher and air permeability 10 times higher than pure PUR membranes. Increasing the concentration above 5 wt.% hindered the spinning process.

Another goal of this work was to clarify the relationships between the technology and structural properties for the design of functional nanofibrous membranes, which meant solving the interactions of nanofibers with additives at the molecular level. During the gradual resolution of these set goals, the following conclusions were found:

The amount of modifying agent used in the spinning solution, i.e., the amount of substances interacting with each other, affects not only the modified membranes but also the spinning process itself. Too high of a concentration leads to defects in the membrane structure (defects of spheres and fibers fused into layers) and could hinder the spinning process itself. Too high of a concentration of some additives leads to a decrease in porosity and air permeability and could result in a decrease in functionality. Too high of an additive concentration could lead to the crystallization of the additive, which happened in our case for PUR/TETA (5 wt.%).

Furthermore, TETA and TEPA substances were found to exhibit different behaviors during the electrospinning process. The TETA amine with a shorter monomer chain tended to crystallize at higher concentrations, and these crystallites were observable in the diffraction pattern for the PUR/TETA (5 wt.%) sample. The crystallization of TETA subsequently affected the properties of the PUR/TETA (5 wt.%) membrane. First, it increased the surface roughness and the inhomogeneous distribution of TETA on the fiber surfaces. Second, it reduced the sorption capacities. On the other hand, the TEPA amines did not crystallize during the spinning process; the amine molecules covered the fiber surface more homogeneously and up to 5 wt.% TEPA, the spinning solution behaved as expected.

These present results confirmed the intermolecular interactions as the key parameters for the structure, morphology, and properties of the electrospun nanofibrous membrane for the design of chemically-modified nanofibrous membranes prepared by electrospinning with a one-step technology. Depending on these mutual intermolecular interactions, we generally observed the following:

A strong tendency of the modifying agent to crystallize, which resulted in the inhomogeneous distribution of the modifying substance on the fiber surfaces. Crystallites were usually observed with the XRD analysis.

On the other hand, the strong polymer-modifier interaction prevented polymer crystallization and led to thinner fibers than in the case of pure polymer spinning.

Another effect of the strong interactions of the molecules of the modifying substances was the sticking of modified nanofibers into bundles, as was observed in the case of the PUR/TEPA samples.

This work confirms the influence of mutual intermolecular interactions on the structure and properties of chemically-modified membranes and shows the usefulness of computer design in the case of chemically-modified nanofibrous membranes. The technology proposed in this work is easily transferable to industrial production lines. On the other hand, even the technology used by us has its limits, which were achieved in this work, so future research must be focused on modifying the spinning technology so that we can prepare porous nanofibers with a rough surface using special additives dissolved in the spinning solution to increase the total surface area of the fibers. We would still be looking for single-stage technology and reasonable air permeability.

Author Contributions: Conceptualization, J.H., P.Č. and P.R.; methodology, J.H. and P.Č.; software, J.T.; validation, J.H., P.Č., M.V., P.R., P.K., J.T., O.B. and V.B.; formal analysis, J.H., M.V., P.R., P.K., J.T. and O.B.; investigation, J.H., P.Č., M.V., P.R., P.K., J.T. and O.B.; resources, P.Č. and O.B.; data curation, J.H. and P.Č.; writing—original draft preparation, J.H.; writing—review and editing, J.H. and P.Č.; visualization, J.H.; supervision, P.Č.; project administration, P.Č.; funding acquisition, P.Č. All authors have read and agreed to the published version of the manuscript.

Funding: This research was funded by the Technology Agency of the Czech Republic, under the project Metamorph, project No. TO01000329, project Research Infrastructure NanoEnviCz, supported by the Ministry of Education, Youth and Sports of the Czech Republic under project NanoEnviCz (No. LM2018124), project SGS No. UJEP-SGS-2022-53-006-3, a project by the Czech Science Foundation [GAČR, no. 20-01639S] and project ERDF/ESF “UniQSurf—Centre of biointerfaces and hybrid functional materials” (No. CZ.02.1.01/0.0/0.0/17_048/0007411).

Data Availability Statement: Not applicable.

Acknowledgments: The authors acknowledge the assistance provided by the Technology Agency of the Czech Republic under the project Metamorph, project No. TO01000329, project Research Infrastructure NanoEnviCz, supported by the Ministry of Education, Youth and Sports of the Czech Republic under project NanoEnviCz (No. LM2018124), project SGS No. UJEP-SGS-2022-53-006-3, a project by the Czech Science Foundation [GAČR, no. 20-01639S] and project ERDF/ESF “UniQSurf—Centre of biointerfaces and hybrid functional materials” (No. CZ.02.1.01/0.0/0.0/17_048/0007411). The authors gratefully acknowledge the access to the electron microscopy facility of IMIC, supported by the Czech Science Foundation grant no. 22-06771S.

Conflicts of Interest: The authors declare that they have no competing interest. The funders had no role in the design of the study, the collection, analyses, and interpretation of data, the writing of the manuscript, or in the decision to publish the results.

References

1. Mills, B.J.; Krause, A.J.; Scotese, C.R.; Hill, D.J.; Shields, G.A.; Lenton, T.M. Modelling the long-term carbon cycle, atmospheric CO₂, and Earth surface temperature from late Neoproterozoic to present day. *Gondwana Res.* **2018**, *67*, 172–186. [[CrossRef](#)]
2. Kweku, D.W.; Bismark, O.; Maxwell, A.; Desmond, K.A.; Danso, K.B.; Oti-Mensah, E.A.; Quachie, A.T.; Adormaa, B.B. Greenhouse Effect: Greenhouse Gases and Their Impact on Global Warming. *J. Sci. Res. Rep.* **2018**, *17*, 1–9. [[CrossRef](#)]
3. Tan, X.; Liu, Y.; Dong, H.; Xiao, Y.; Zhao, Z. The health consequences of greenhouse gas emissions: A potential pathway. *Environ. Geochem. Health* **2022**, *44*, 2955–2974. [[CrossRef](#)] [[PubMed](#)]
4. Song, C.; Liu, Q.; Ji, N.; Deng, S.; Zhao, J.; Li, Y.; Song, Y.; Li, H. Alternative pathways for efficient CO₂ capture by hybrid processes—A review. *Renew. Sustain. Energy Rev.* **2017**, *82*, 215–231. [[CrossRef](#)]
5. Sanni, E.S.; Sadiku, E.R.; Okoro, E.E. Novel Systems and Membrane Technologies for Carbon Capture. *Int. J. Chem. Eng.* **2021**, *2021*, 6642906. [[CrossRef](#)]
6. Al-Mamoori, A.; Rownaghi, A.A.; Rezaei, F. Carbon Capture and Utilization Update. *Energy Technol.* **2017**, *5*, 834–849. [[CrossRef](#)]
7. Drioli, E.; Barbieri, G.; Brunetti, A. Membrane Engineering for the Treatment of Gases: Volume 1: Gas-separation Problems with Membranes. In *Recent High Performance Polymer Membranes for CO₂ Separation*; The Royal Society of Chemistry: London, UK, 2011; Volume 1, pp. 84–124.
8. Vopička, O.; de Angelis, M.G.; Sarti, G.C. Mixed gas sorption in glassy polymeric membranes: I. CO₂/CH₄ and n-C₄/CH₄ mixtures sorption in poly(1-trimethylsilyl-1-propyne) (PTMSP). *J. Membr. Sci.* **2014**, *449*, 97–108. [[CrossRef](#)]
9. Kim, H.; Lee, K.S. Energy analysis of an absorption-based CO₂ capture process. *Int. J. Greenh. Gas Control* **2017**, *56*, 250–260. [[CrossRef](#)]
10. Rochelle, G.T. Amine Scrubbing for CO₂ Capture. *Science* **2009**, *325*, 1652–1654. [[CrossRef](#)]
11. Ho, M.T.; Allinson, G.W.; Wiley, D.E. Reducing the Cost of CO₂ Capture from Flue Gases Using Membrane Technology. *Ind. Eng. Chem. Res.* **2008**, *47*, 1562–1568. [[CrossRef](#)]
12. Zainab, G.; Babar, A.A.; Iqbal, N.; Wang, X.; Yu, J.; Ding, B. Amine-impregnated porous nanofiber membranes for CO₂ capture. *Compos. Commun.* **2018**, *10*, 45–51. [[CrossRef](#)]
13. Abbasi, A.; Nasef, M.M.; Kheawhom, S.; Faridi-Majidi, R.; Takeshi, M.; Abouzari-Lotf, E.; Choong, T. Amine functionalized radiation induced grafted polyolefin nanofibers for CO₂ adsorption. *Radiat. Phys. Chem.* **2018**, *156*, 58–66. [[CrossRef](#)]
14. Nasef, M.M.; Ting, T.; Abbasi, A.; Layeghi-Moghaddam, A.; Alinezhad, S.S.; Hashim, K. Radiation grafted adsorbents for newly emerging environmental applications. *Radiat. Phys. Chem.* **2016**, *118*, 55–60. [[CrossRef](#)]
15. Zainab, G.; Iqbal, N.; Babar, A.A.; Huang, C.; Wang, X.; Yu, J.; Ding, B. Free-standing, spider-web-like polyamide/carbon nanotube composite nanofibrous membrane impregnated with polyethyleneimine for CO₂ capture. *Compos. Commun.* **2017**, *6*, 41–47. [[CrossRef](#)]
16. Wang, J.; Adelodun, A.A.; Oh, J.M.; Jo, Y.M. TEPA impregnation of electrospun carbon nanofibers for enhanced low-level CO₂ adsorption. *Nano Converg.* **2020**, *7*, 7. [[CrossRef](#)]
17. Wang, X.; Li, B. Electrospun Nanofibrous Sorbents and Membranes for Carbon Dioxide Capture. In *Electrospun Nanofibers for Energy and Environmental Applications*; Ding, B., Yu, J., Eds.; Springer: Berlin/Heidelberg, Germany, 2014; pp. 249–263.
18. Choi, C.; Kadam, R.L.; Gaikwad, S.; Hwang, K.-S.; Han, S. Metal organic frameworks immobilized polyacrylonitrile fiber mats with polyethyleneimine impregnation for CO₂ capture. *Microporous Mesoporous Mater.* **2020**, *296*, 110006. [[CrossRef](#)]

19. Othman, F.E.C.; Yusof, N.; Petru, M.; Nordin, N.A.H.M.; Hamid, M.F.; Ismail, A.F.; Rushdan, A.I.; Abu Hassan, S. Polyethyleneimine-impregnated activated carbon nanofiber composited graphene-derived rice husk char for efficient post-combustion CO₂ capture. *Nanotechnol. Rev.* **2022**, *11*, 926–944. [[CrossRef](#)]
20. Heo, Y.-J.; Zhang, Y.; Rhee, K.Y.; Park, S.-J. Synthesis of PAN/PVDF nanofiber composites-based carbon adsorbents for CO₂ capture. *Compos. Part B Eng.* **2018**, *156*, 95–99. [[CrossRef](#)]
21. Chiang, Y.-C.; Wu, C.-Y.; Chen, Y.-J. Effects of activation on the properties of electrospun carbon nanofibers and their adsorption performance for carbon dioxide. *Sep. Purif. Technol.* **2019**, *233*, 116040. [[CrossRef](#)]
22. Iqbal, N.; Babar, A.A.; Zainab, G.; Ding, B.; Yu, J.; Wang, X. Chapter 20—Electrospun Nanofibers for Carbon Dioxide Capture. In *Electrospinning: Nanofabrication and Applications*; Ding, B., Wang, X., Yu, J., Eds.; William Andrew Publishing: Norwich, NY, USA, 2019; pp. 619–640.
23. Jung, H.; Jo, D.H.; Lee, C.H.; Chung, W.; Shin, D.; Kim, S.H. Carbon Dioxide Capture Using Poly(ethylenimine)-Impregnated Poly(methyl methacrylate)-Supported Sorbents. *Energy Fuels* **2014**, *28*, 3994–4001. [[CrossRef](#)]
24. Jung, H.; Lee, C.H.; Jeon, S.; Jo, D.H.; Huh, J.; Kim, S.H. Effect of amine double-functionalization on CO₂ adsorption behaviors of silica gel-supported adsorbents. *Adsorption* **2016**, *22*, 1137–1146. [[CrossRef](#)]
25. Kludský, M.; Vopička, O.; Matějka, P.; Hovorka, Š.; Friess, K. Nafion® modified with primary amines: Chemical structure, sorption properties and pervaporative separation of methanol-dimethyl carbonate mixtures. *Eur. Polym. J.* **2018**, *99*, 268–276. [[CrossRef](#)]
26. Kuang, Y.; He, H.; Chen, S.; Wu, J.; Liu, F. Adsorption behavior of CO₂ on amine-functionalized polyacrylonitrile fiber. *Adsorption* **2019**, *25*, 693–701. [[CrossRef](#)]
27. Lin, Z.F.; Wei, J.W. CO₂ Adsorption on Activated Carbon/SBA-15 with TETA/TEPA Modification. *Key Eng. Mater.* **2017**, *735*, 164–167. [[CrossRef](#)]
28. Ma, L.; Bai, R.; Hu, G.; Chen, R.; Hu, X.; Dai, W.; Dacosta, H.F.M.; Fan, M. Capturing CO₂ with Amine-Impregnated Titanium Oxides. *Energy Fuels* **2013**, *27*, 5433–5439. [[CrossRef](#)]
29. Qing, Y.; Yu, Z.; Ming, L.; Yao, S. Adsorption of Low Concentration CO₂ by Modified Carbon Nanotubes under Ambient Temperature. *Acta Phys.-Chim. Sin.* **2012**, *28*, 1223–1229. [[CrossRef](#)]
30. Wei, J.; Lin, Z.; He, Z.; Geng, L.; Liao, L. Bagasse Activated Carbon with TETA/TEPA Modification and Adsorption Properties of CO₂. *Water Air Soil Pollut.* **2017**, *228*, 128. [[CrossRef](#)]
31. Zhang, J.; Zhao, Q.; Wang, S.; Tan, X. Direct capture of low concentration CO₂ using tetraethylenepentamine-grafted polyacrylonitrile hollow fibers. *Sep. Purif. Technol.* **2022**, *287*, 120562. [[CrossRef](#)]
32. Jiao, J.; Cao, J.; Xia, Y.; Zhao, L. Improvement of adsorbent materials for CO₂ capture by amine functionalized mesoporous silica with worm-hole framework structure. *Chem. Eng. J.* **2016**, *306*, 9–16. [[CrossRef](#)]
33. Kim, T.-J.; Li, B.; Hägg, M.-B. Novel fixed-site-carrier polyvinylamine membrane for carbon dioxide capture. *J. Polym. Sci. Part B Polym. Phys.* **2004**, *42*, 4326–4336. [[CrossRef](#)]
34. Kim, S.; Lee, Y.M. High performance polymer membranes for CO₂ separation. *Curr. Opin. Chem. Eng.* **2013**, *2*, 238–244. [[CrossRef](#)]
35. Zhao, L.; Weber, M.; Stolten, D. Comparative Investigation of Polymer Membranes for Post-combustion Capture. *Energy Procedia* **2013**, *37*, 1125–1134. [[CrossRef](#)]
36. Tong, Z.; Ho, W.W. New sterically hindered polyvinylamine membranes for CO₂ separation and capture. *J. Membr. Sci.* **2017**, *543*, 202–211. [[CrossRef](#)]
37. Bai, F.; Liu, X.; Sani, S.; Liu, Y.; Guo, W.; Sun, C. Amine functionalized mesocellular silica foam as highly efficient sorbents for CO₂ capture. *Sep. Purif. Technol.* **2022**, *299*, 121539. [[CrossRef](#)]
38. Anyanwu, J.-T.; Wang, Y.; Yang, R.T. Tunable amine loading of amine grafted mesoporous silica grafted at room temperature: Applications for CO₂ capture. *Chem. Eng. Sci.* **2022**, *254*, 117626. [[CrossRef](#)]
39. Sharmin, E.; Zafar, F. Polyurethane: An Introduction. In *Polyurethane*, 1st ed.; Zafar, F., Sharmin, E., Eds.; InTech: Rijeka, Croatia, 2012; pp. 3–6.
40. Das, A.; Mahanwar, P. A brief discussion on advances in polyurethane applications. *Adv. Ind. Eng. Polym. Res.* **2020**, *3*, 93–101. [[CrossRef](#)]
41. Jirsak, O.; Sanetnik, F.; Lukas, D.; Kotek, V.; Martinova, L.; Chaloupek, J. Method of Nanofibres Production from A Polymer Solution Using Electrostatic Spinning and A Device for Carrying out the Method. U.S. Patent 7585437B2, 8 September 2009.
42. Ibrahim, H.M.; Klingner, A. A review on electrospun polymeric nanofibers: Production parameters and potential applications. *Polym. Test.* **2020**, *90*, 106647. [[CrossRef](#)]
43. Schindelin, J.; Arganda-Carreras, I.; Frise, E.; Kaynig, V.; Longair, M.; Pietzsch, T.; Preibisch, S.; Rueden, C.; Saalfeld, S.; Schmid, B.; et al. Fiji: An open-source platform for biological-image analysis. *Nat. Methods* **2012**, *9*, 676–682. [[CrossRef](#)]
44. Benkocká, M.; Kolářová, K.; Matoušek, J.; Semerádtová, A.; Šícha, V.; Kolská, Z. Nanocomposite of polystyrene foil grafted with metallaboranes for antimicrobial activity. *Appl. Surf. Sci.* **2018**, *441*, 120–129. [[CrossRef](#)]
45. Benkocká, M.; Lupínková, S.; Matoušek, J.; Kolářová, K.; Kolská, Z. Antimicrobial and optical properties of PET chemically modified and grafted with borane compounds. *RSC Adv.* **2018**, *8*, 15001–15008. [[CrossRef](#)]
46. Kolská, Z.; Kasálková, N.S.; Siegel, J.; Švorčík, V. Electrokinetic Potential for Characterization of Nanostructured Solid Flat Surfaces. *J. Nano Res.* **2013**, *25*, 31–39. [[CrossRef](#)]
47. Kolská, Z.; Řezníčková, A.; Svorcik, V. Surface characterization of polymer foils. *e-Polymers* **2012**, *12*, 960–972. [[CrossRef](#)]

48. Sun, H. COMPASS: An ab Initio Force-Field Optimized for Condensed-Phase Applications Overview with Details on Alkane and Benzene Compounds. *J. Phys. Chem. B* **1998**, *102*, 7338–7364. [[CrossRef](#)]
49. Ryšánek, P.; Čapková, P.; Štojd, J.; Trögl, J.; Benada, O.; Kormunda, M.; Kolská, Z.; Munzarová, M. Stability of antibacterial modification of nanofibrous PA6/DTAB membrane during air filtration. *Mater. Sci. Eng. C* **2018**, *96*, 807–813. [[CrossRef](#)] [[PubMed](#)]
50. Čapková, P.; Kormunda, M.; Kolská, Z.; Trögl, J.; Munzarová, M.; Ryšánek, P. Electrospun Antimicrobial PVDF-DTAB Nanofibrous Membrane for Air Filtration: Effect of DTAB on Structure, Morphology, Adhesion, and Antibacterial Properties. *Macromol. Mater. Eng.* **2018**, *303*, 1700415. [[CrossRef](#)]
51. Ryšánek, P.; Malý, M.; Čapková, P.; Kormunda, M.; Kolská, Z.; Gryndler, M.; Novák, O.; Hocelíková, L.; Bystrianský, L.; Munzarová, M. Antibacterial modification of nylon-6 nanofibers: Structure, properties and antibacterial activity. *J. Polym. Res.* **2017**, *24*, 208. [[CrossRef](#)]
52. Marin, L.; Dragoi, B.; Olaru, N.; Perju, E.; Coroaba, A.; Doroftei, F.; Scavia, G.; Destri, S.; Zappia, S.; Porzio, W. Nanoporous furfuryl-imine-chitosan fibers as a new pathway towards eco-materials for CO₂ adsorption. *Eur. Polym. J.* **2019**, *120*, 109214. [[CrossRef](#)]
53. Imanian, Z.; Hormozi, F.; Torab-Mostaedi, M.; Asadollahzadeh, M. Highly selective adsorbent by gamma radiation-induced grafting of glycidyl methacrylate on polyacrylonitrile/polyurethane nanofiber: Evaluation of CO₂ capture. *Sep. Purif. Technol.* **2022**, *289*, 120749. [[CrossRef](#)]
54. Zheng, W.; Li, Z.; Sun, T.; Ruan, X.; Dai, Y.; Li, X.; Zhang, C.; He, G. PAN electrospun nanofiber skeleton induced MOFs continuous distribution in MMMs to boost CO₂ capture. *J. Membr. Sci.* **2022**, *650*, 120330. [[CrossRef](#)]